〈制导与对抗〉

Strategy of Barrel Roll and Decoy Deployment Against Infrared Air-to-Air Missile

ZHANG Nan[1]，CHEN Changsheng[1]，SUN Jingguo[1]，LIANG Xuechao[2]

(1. *Aeronautics Computing Technology Research Institute, Xi'an* 710065, *China*;
2. *China Academy of Launch Vehicle Technology, Beijing* 100076, *China*)

Abstract：Evasive maneuvers and decoy deployment are effective measures against infrared (IR) air-to-air missiles for fighters. In this study, both aspects were considered: barrel roll maneuver and unpowered point source decoys. For practical purposes, the interference process, movement characteristics, and influence mechanism of the decoy on the missile guidance system are expounded, in which the conditions needed for the barrel roll maneuver and the force of the decoy are considered. In addition, the air-to-air missile is assumed to adopt the true proportional navigation law or augmented proportional navigation law, and the decoys are launched in the conventional mode or emergency mode. Linearized time-varying models and adjoint models for barrel roll maneuvers with decoy deployment influence on missile guidance precision are established. The correctness of these models was verified by a simulation result analysis and comparison. The miss distance is an important parameter for characterizing the performance of an air-defense missile. The average miss distance and percentage of maximum miss distance were proposed to analyze the adjoint model results. Based on the work mentioned above, the barrel roll rate and the transition step maneuver angle of the target aircraft, as well as the simultaneous launch quantity, the period between successive launches, and launch direction policy on the miss distance are analyzed to provide strategic references for fighters against IR air-to-air missiles.

Key words: adjoint method, decoy launch, evasive maneuver, IR air-to-air missile, miss distance, proportional navigation law

基于桶滚机动和诱饵投射的红外空空导弹对抗策略研究

张 楠[1]，陈长胜[1]，孙靖国[1]，梁雪超[2]

（1. 中国航空工业计算所，陕西 西安 710065；2. 中国运载火箭技术研究院，北京 100076）

摘要：机动规避和投射诱饵是战斗机对抗红外空对空导弹的有效措施。本文主要从桶滚机动和无动力型点源诱饵两方面进行了对抗策略研究。为了使研究更具实用性，在考虑桶滚机动所需条件和诱饵弹受力的前提下，阐述了诱饵弹的运动特性、干扰过程和对导弹制导系统的影响机理。为使研究更具适用性，本文假设空对空导弹采用真比例导引律或增广比例导引律，并且诱饵考虑在常规模式和应急模式下投射。建立了桶滚机动并伴有诱饵投射时对导弹制导精度影响的线性化时变模型和伴随模型。同时，通过仿真结果的分析与比较，验证了模型的正确性。脱靶量是表征防空导弹性能的一个重要参数，提出了平均脱靶量和最大脱靶量占比来分析伴随模型的仿真结果。在此基础上，分析了目标机的桶滚机动角速率和过渡机动方位角以及诱饵弹的齐投数量、投射间隔与投射方向策略对导弹脱靶量的影响规律。这将为战斗机对抗红外空对空导弹提供策略参考。

关键词：伴随法；诱饵投射；机动规避；红外空空导弹；脱靶量；比例导引律

中图分类号：TJ765.3 **文献标识码**：A **文章编号**：1001-8891(2022)03-0231-13

Received date：2021-08-02；**Revised date**：2021-09-23.

Biography：ZHANG Nan (1987-), Male, Xi'an Shaanxi, Master degree, Mainly engaged in the research of avionics bus network and guidance. E-mail: 550100308@qq.com.

0 Introduction

Compared with radar air-to-air missiles, infrared (IR) air-to-air missiles have a strong anti-interference ability and high hit rate and are widely used in air combat. History suggests that almost 90% of all downed aircraft between 1979 and 1993 were destroyed by IR-homing missiles. In addition, 14 out of 22 airplanes (78%) were downed by IR homing missiles during the First Gulf War [1]. IR air-to-air missiles are the most effective short-range air combat weapons. Therefore, it is necessary to study countermeasures against IR air-to-air missiles.

Short-range IR air-to-air missiles mainly pursue the target using proportional navigation (PN) [2-3] or its modified forms [4-5]. PN has been widely used in engineering because of its straight terminal trajectory, small overload, strong robustness, and high precision. PN can be used as long as line-of-sight (LOS) can be acquired. PN guidance laws can be categorized into two major classes [6]. The first is missile velocity referenced PNs, which mainly include pure proportional navigation (PPN) and its variants, where the commanded acceleration is perpendicular to the missile velocity. Suwon Lee et al. [7] performed a statistical analysis of the missile's capture region for pure proportional navigation guidance considering target maneuvers. LI Kebo et al. [8] proposed a guidance strategy with impact angle constraints based on PPN and the interception performance was demonstrated through numerical simulation examples. Satadal Ghosh et al. [9] proposed a composite proportional navigation guidance law using a combination of standard pure proportional navigation and the retro-proportional navigation guidance laws for intercepting higher speed non-maneuvering targets at specified impact angles in three-dimensional engagements. The second class of PNs is LOS referenced PNs, including true proportional navigation (TPN) and its variants. The performance of 3D TPN against an arbitrarily maneuvering target was thoroughly analyzed using the Lyapunov-like approach by LI Kebo et al. [10], and, the upper bound of the 3D LOS rate and the commanded acceleration of the 3D TPN were obtained. Feng Tyan [11] analyzed the capture area of general 3D TPN guidance laws using a novel method. A more practical capture region of the realistic true proportional navigation guidance law for an arbitrarily maneuvering target was analyzed by BAI Zhihui et al. [12]. The direction of the TPN's commanded acceleration was perpendicular to the LOS, and its magnitude was only proportional to the LOS rate. When aiming at a maneuvering target, if the target maneuver compensation is added to the proportional navigation, it is called augmented proportional navigation (APN). According to the optimal control theory, it can be proved that PN is the optimal solution of the linear guidance problem that minimizes the square integral of the control quantity without considering the target's maneuvers or the dynamic delay of the guidance system. APN is the optimal guidance navigation for a maneuvering target with a constant overload. The missiles used in this study were considered to have adopted these two guidance laws.

The target aircraft mainly avoids attacks from IR air-to-air missiles by implementing tactical maneuvers [13] and IR interference [1,14]. The numerically obtained three-dimensional optimal evasive maneuvers of a fighter against a proportional navigation missile are those of the vertical-S type and horizontal-S type [15], which are two-dimensional in nature. The barrel roll maneuver is regarded as an approximation of these optimal maneuvers; however, the barrel roll maneuver is easier to implement than the optimal maneuvers [16]. The barrel roll maneuver is an effective maneuvering form [17].

According to the radiation characteristics of IR decoys, the decoys can be divided into point source decoys and surface decoys. According to their motion characteristics, IR decoys can be divided into unpowered, aerodynamic, self-propelled, towered, and air-launched decoys. Most research on IR decoys focuses on compositions [18], simulations [19], IR target recognition algorithms [20-21], and so on. This paper focuses on the deployment policy of the unpowered point source decoy considering the influence on the missile miss distance from the guidance point of view, and thus, target recognition is reasonably simplified.

In terms of research methods, the adjoint method is widely used for missile modeling and simulation, performance evaluation, precision analysis of guidance system, and other problems such as target allocation. Among them, Martin Weiss et al. introduced the adjoint method for state space models [22], hybrid guidance loop state-space models [23] and two-phase guidance loop

models [24]. LI Quancheng et al. [25] presented three seeker blind range guidance policies with different guidance precisions using the adjoint method. Several computationally efficient weapon target-allocation algorithms for assigning defenders to missiles in a cooperative interception scenario were developed by Vitaly Shalumov et al. [26]. Domenic Bucco and Martin Weiss [27] used the adjoint method to study the influence of the blind range of seekers on missile guidance. Timo Sailaranta et al. [17] established a simple model of the target barrel roll maneuver, and validated its rationality using the adjoint method. However, none of the above studies considered the influence of decoy deployment on the miss distance of the missiles. WANG Weiqiang et al. [28] proposed a guidance precision analysis method for the entir process of air countermeasures from infrared decoy deployment, identification, and guidance disturbance to the final miss distance calculation. Arthur Vermeulen et al. [29] used the adjoint method to study the influence of the target maneuver and decoy interference on the miss distance of the missile and provided corresponding countermeasures; however, they studied the two-dimensional maneuver of the target and did not consider the effect of the decoy force. Huang Hesong et al. [30] established the movement and radiation models of target maneuver and surface-type decoy based on real data, and the best defense strategy was analyzed when the missile came from the front of the aircraft, however there was little work on a multi-decoy deployment policy.

In this study, considering the interference process, movement characteristics, and influence mechanism of the decoy on the missile guidance system, mathematical models to study the tactical strategy of the target barrel roll maneuver and decoy deployment against an infrared air-to-air missile were proposed based on the adjoint method. The main contributions of this study are as follows:

1) The model built in this study comprehensively considers the barrel roll maneuver and decoy deployment, which are closer to the actual situation, and fully validates the model. The modeling method can provide a reference for other maneuver forms and decoy deployment research.

2) Maneuver and decoy deployment strategies are usually studied from an experimental point of view, which requires a large amount of work and lacks regularity. In contrast, computational efficiency can be improved, and more rules can be found with the introduction of the adjoint method.

3) The target and decoy of this study are built in an absolute coordinate system, which can not only can model and analyze the conventional deployment mode but also the emergency deployment mode.

4) The miss distance is considered an important index of missile combat performance. The average miss distance and percentage of maximum miss distance, which considers the occurrence probability of time-to-go, are proposed to analyze the results of the adjoint model.

The remainder of this paper is organized as follows. The decoy interference processes are described in Section 1. The linearized time-varying models and adjoint analysis models for barrel roll maneuvers with decoy deployment influence on the missile guidance precision are established in Section 2. Section 3 presents model validation, simulation results, and analysis. Finally, conclusions are presented in Section 4.

1 Description and modeling of decoy interference process

The classical decoy interference process in this study is described as follows: when the decoy is launched, a radiation source similar to the target IR characteristic is generated in the seeker's field of view. Without loss of generality, we can assume that the LOS of the missile is no longer aimed at the target, but at the power centroid of the target and the decoys until the target has been identified. This type of interference is called power centroid interference. Suppose that the position, velocity, and acceleration for the i-th decoy in the seeker field of view are (y_{Di}, z_{Di}), (V_{Dyi}, V_{Dzi}) and (a_{Dyi}, a_{Dzi}), respectively. While (y_T, z_T), (V_{Ty}, V_{Tz}) and (a_{Ty}, a_{Tz}) are the position, velocity, and acceleration of the target, respectively. W_T denotes the radiation intensity of the target. Then, the position y_C, velocity V_{Cy} and acceleration a_{Cy} of the power centroid in the Y-direction can be calculated as:

$$\begin{cases} y_C = \dfrac{W_T y_T + W_{D1} y_{D1} + \cdots + W_{Di} y_{Di} + \cdots}{W_T + W_{D1} + \cdots + W_{Di} + \cdots} \\ V_{Cy} = \dfrac{W_T V_{y_T} + W_{D1} V_{y_{D1}} + \cdots + W_{Di} V_{y_{Di}} + \cdots}{W_T + W_{D1} + \cdots + W_{Di} + \cdots} \\ a_{Cy} = \dfrac{W_T a_{y_T} + W_{D1} a_{y_{D1}} + \cdots + W_{Di} a_{y_{Di}} + \cdots}{W_T + W_{D1} + \cdots + W_{Di} + \cdots} \end{cases} \quad (1)$$

The corresponding physical quantity of the power centroid in the *Z*-direction is similar to that in (1). The technical parameters involved include simultaneous launch quantity, the period between successive launches, and launch direction policy.

The missile anti-interference process can be described in three phases [29], as shown in Fig. 1.

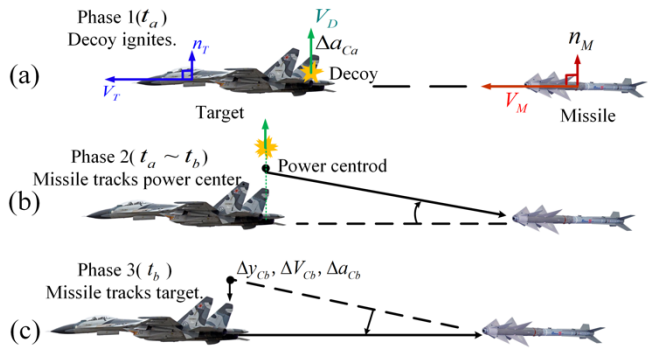

Fig. 1 The process of air-to-air missile anti-interference

In the missile's terminal guidance, the seeker locks and tracks the target and the target launches the decoy at t_a. The decoy ignites and leaves the target, as shown in Fig. 1 (a), corresponding to the first phase. The lateral position of the decoy is consistent with that of the aircraft; however, their lateral accelerations and velocities are different. Because the missile seeker cannot instantaneously discriminate between the decoy and target, the seeker tracks the power centroid, that is, the false target. With the movements of the decoy and target, the false target moves away from the aircraft, and the seeker tracks it during the period of time t_a to t_b, as shown in Fig. 1(b), corresponding to the second phase. After the discrimination time, the seeker has successfully discriminated the target through the anti-interference algorithm of the seeker at t_b, which means the missile begins to track the target (assuming that the target is still in the seeker's field of view) and the aiming point instantly shifts back to the target, as shown in Fig.1(c) corresponding to the third phase. If the target has already left the seeker's field of view, then the seeker will lose the target, which is not discussed in this paper. In the figure, V_M and V_T represent the constant velocities of the missile and target, respectively. V_c represents the closing speed of the missile and the target. For the head-on scenario, $V_c = V_M + V_T$, and for tail chase, $V_c = V_M - V_T$. For simplicity, the initial value of the LOS angle was taken as zero, that is, $q = 0$. The time-to-go $t_{go} = t_F - t$, where t_F is the final time of the engagement corresponding to the minimal miss distance and t is the current flight time. The distance between the missile and the target, R, is given by the product of V_c and t_{go}. n_M and n_T are taken as the maneuver overloads of the missile and target, respectively. V_D denotes the decoy velocity. Δy_{Cb}, ΔV_{Cb} and Δa_{Cb} are the suddenly shifted values of the displacement, velocity, and acceleration of the power centroid, respectively, at t_b.

To induce an IR-guided air-to-air missile effectively, the radiation intensity of the decoy is always designed to be higher than the IR radiation intensity of the aircraft. The ratio of the decoy radiation energy to the target radiation energy in the dynamic state, that is, the suppression coefficient K, is generally between 2 and 3. It can be considered that the intensity of the IR radiation source formed by multiple decoys launched by the target in each group is the sum of the radiation intensity of every single decoy. Here, we consider the radiation intensity of the decoy to be the same and equal to W_D. Thus, K can be calculated as

$$K = W_D / W_T \tag{2}$$

2 Models of Target Maneuver and Decoy Deployment Influence on Missile

2.1 Model of target maneuver

The model described in [17] considers that the aircraft barrel roll maneuver has a certain normal velocity, however the normal situation is that the target aircraft is in a cruising state; that is, the target is in a uniform straight flight state when the missile is launched. The target first implements a step-transition maneuver that utilizes the rated overload capacity, then the barrel roll will be implemented. Fig. 2 shows a schematic of the barrel roll maneuver. The maneuver was as follows: the target flew with a circular motion in the plumb plane and moved at a uniform speed along the axle of the barrel roll. The origin of the coordinate system is the barrel roll axis.

ϕ_0 and ω denote the initial phase angle and the barrel roll rate, respectively. The initial velocity of the target barrel roll *is* $V_R = a_T/\omega = n_T g/\omega$, and the time spent on the step maneuver is $t_{step} = V_R/a_T = 1/\omega$. $\psi_0 = \phi_0 + \pi/2$ is the angle of the step maneuver. n_{Ty}, n_{Tz}, a_{Ty}, and a_{Tz} are the overload and acceleration values of the target in the Y and

Z directions, respectively, which can be calculated during the step maneuver as follows:

$$\begin{cases} a_{\mathrm{T}y} = n_{\mathrm{T}y} g = n_{\mathrm{T}} g \sin(\psi_0) & t \le t_{\mathrm{step}} \\ a_{\mathrm{T}z} = n_{\mathrm{T}z} g = n_{\mathrm{T}} g \cos(\psi_0) & t \le t_{\mathrm{step}} \end{cases} \tag{3}$$

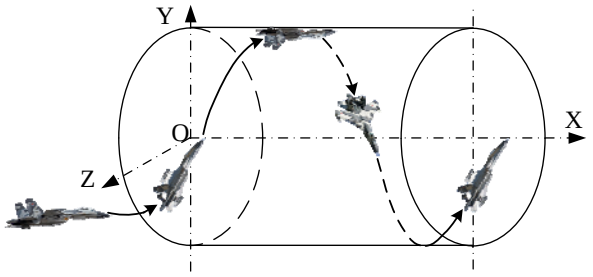

Fig. 2 Schematic diagram of barrel roll maneuver

Whereas overload and acceleration value of target during barrel roll can be given by

$$\begin{cases} a_{\mathrm{T}y} = n_{\mathrm{T}y} g = -n_{\mathrm{T}} g \sin[\omega(t - t_{\mathrm{step}}) + \phi_0] & t > t_{\mathrm{step}} \\ a_{\mathrm{T}z} = n_{\mathrm{T}z} g = -n_{\mathrm{T}} g \cos[\omega(t - t_{\mathrm{step}}) + \phi_0] & t > t_{\mathrm{step}} \end{cases} \tag{4}$$

According to the definition in Fig. 2 and the origin of the coordinate system, the initial *Y* and *Z* coordinates of the targets $y_{\mathrm{T}0}$ and $z_{\mathrm{T}0}$ are

$$\begin{cases} y_{\mathrm{T}0} = -1/2 n_{\mathrm{T}} g t_{\mathrm{step}}^2 \sin\psi_0 + R\sin\phi_0 \\ z_{\mathrm{T}0} = -1/2 n_{\mathrm{T}} g t_{\mathrm{step}}^2 \cos\psi_0 + R\cos\phi_0 \end{cases} \tag{5}$$

And the position of the target in the simulation can be calculated as

$$\begin{cases} y_{\mathrm{T}} = \begin{cases} 1/2 n_{\mathrm{T}} g (t^2 - t_{\mathrm{step}}^2)\sin\psi_0 + R\sin\phi_0, & t \leqslant t_{\mathrm{step}} \\ R\sin(\phi_0 + \omega(t - t_{\mathrm{step}})), & t > t_{\mathrm{step}} \end{cases} \\ z_{\mathrm{T}} = \begin{cases} 1/2 n_{\mathrm{T}} g (t^2 - t_{\mathrm{step}}^2)\cos\psi_0 + R\cos\phi_0, & t \leqslant t_{step} \\ R\sin(\phi_0 + \omega(t - t_{\mathrm{step}})), & t > t_{\mathrm{step}} \end{cases} \end{cases} \tag{6}$$

The target maneuver can then be transformed into a pulse input function, and the acceleration in the *Y*-direction is shown in Fig. 3.

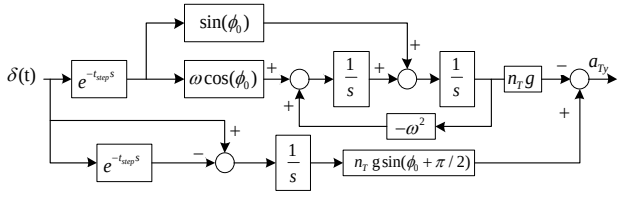

Fig. 3 Pulse input of acceleration signal in the *Y* direction

2.2 Model of IR decoy

The decoy is primarily affected by gravity and aerodynamic drag. The kinematic equations are as follows[30]:

$$\begin{cases} f = 0.5 C_{\mathrm{d}} S \rho V_{\mathrm{D}}^2 \\ m_{\mathrm{D}} \dfrac{\mathrm{d}V_{\mathrm{D}x}}{\mathrm{d}t} = -f \dfrac{V_{\mathrm{D}x}}{V_{\mathrm{D}}} \\ m_{\mathrm{D}} \dfrac{\mathrm{d}V_{\mathrm{D}y}}{\mathrm{d}t} = -f \dfrac{V_{\mathrm{D}y}}{V_{\mathrm{D}}} - m_{\mathrm{D}} g \\ m_{\mathrm{D}} \dfrac{\mathrm{d}V_{\mathrm{D}z}}{\mathrm{d}t} = -f \dfrac{V_{\mathrm{D}z}}{V_D} \end{cases} \tag{7}$$

where ρ is the atmospheric density and *f*, C_{d}, *S*, m_{D}, *and* V_{D} are the drag force, drag coefficient, windward area, mass, and velocity of the decoy, respectively. $V_{\mathrm{D}x}$, $V_{\mathrm{D}y}$, *and* $V_{\mathrm{D}z}$ denote the components of the missile velocity in the coordinate system shown in Fig. 2, and *g* is the gravitational acceleration. This paper discusses the initial velocity of the decoy in the barrel roll maneuver, which can be calculated as follows:

$$\begin{cases} V_{\mathrm{D}x0} = V_{\mathrm{T}x} \\ V_{\mathrm{D}y0} = V_{\mathrm{T}y} + V_{\mathrm{F}} \sin(\phi) \\ V_{\mathrm{D}z0} = V_{\mathrm{T}z} + V_{\mathrm{F}} \cos(\phi) \end{cases} \tag{8}$$

where V_{F} is the launch velocity of the decoy relative to the target aircraft, which is positive when the decoy is launched to the outer side of the circular motion; otherwise, it is negative. ϕ denotes the angle for the barrel roll maneuver during decoy launch.

Taking the *Y*-direction as an example, a decoy model was established, and the *Z*-direction is similar. To facilitate modeling, the decoy acceleration $a_{\mathrm{D}y}$ is considered to be constant in the second phase of Fig. 1. The specific calculation is as follows:

$$a_{\mathrm{D}y} = \frac{V_{\mathrm{D}yb} - V_{\mathrm{D}ya}}{t_{ab}} \tag{9}$$

where $V_{\mathrm{D}ya}$ and $V_{\mathrm{D}yb}$ are the velocities of the decoy in the *Y*-direction at t_a and t_b, respectively. Certainly, $t_{ab}=t_b-t_a$ is the significant time of the decoy, that is, the identification time required by the anti-interference algorithms of the seeker.

2.3 Calculation model of miss distance for IR decoy in conventional launch mode

The conventional launch mode of the IR decoy considered here refers to the launch mode with a period of successive launches not less than the t_{ab}. Other parameters include the simultaneous launch quantity n and the launch direction policy. In actual combat situations, the quantity,

direction, and speed of every decoy causes a difference in the discrimination time of the seeker. In this study, it is assumed that the seeker needs another fixed time to discriminate the real target whenever a new decoy appears in the seeker field of view. By analyzing the anti-interference process of the IR air-to-air missile, as shown in Fig. 1, in the absence of velocity pointing deviation and initial displacement deviation, the influence model of the power centroid under the barrel roll maneuver on the missile miss distance is shown in Fig. 4.

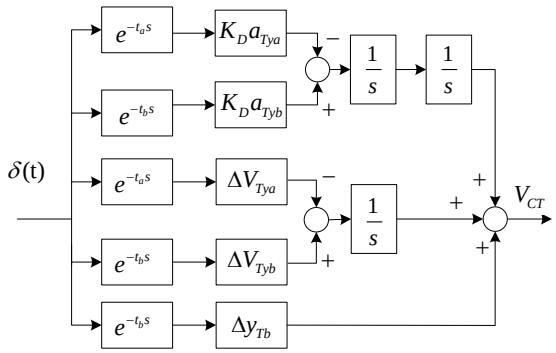

Fig. 4 Influence model of power centroid under barrel roll

In Fig. 4, $K_D = K/(K+1)$ is the sudden shift value and V_{CT} denotes the influence of the target maneuver on the power centroid velocity when the decoy works. According to (1), the effect of the target on the acceleration of the power centroid is decreased by K_D times at t_a, and the effect is increased by K_D times at t_b. Because of the time delay link, the initial phase of the sinusoidal signal needs to be adjusted according to (9) to ensure consistency with the phase at the moment of acceleration shift.

$$\begin{cases} a_{Tya} = -n_T g \sin[\omega(t - t_{step}) + \phi_0 + \omega t_a] \\ a_{Tyb} = -n_T g \sin[\omega(t - t_{step}) + \phi_0 + \omega t_b] \end{cases} \tag{10}$$

ΔV_{Tya} represents the velocity shift value of the power centroid caused by the target maneuver at t_a, whereas ΔV_{Tyb} and Δy_{Tb} represent the velocity and displacement shift values at t_b respectively, which can be calculated as

$$\begin{cases} \Delta V_{Tya} = \begin{cases} K_D V_{Tya} & t \geqslant t_a \\ 0 & t < t_a \end{cases} \\ \Delta V_{Tyb} = \begin{cases} K_D V_{Tyb} & t \geqslant t_b \\ 0 & t < t_b \end{cases} \\ \Delta y_{Tb} = \begin{cases} K_D y_{Tb} & t \geqslant t_b \\ 0 & t < t_b \end{cases} \end{cases} \tag{11}$$

where V_{Tya} represents the velocity of the target at t_a and V_{Tyb} and y_{Tb} represent the velocity and position of the target at t_b, respectively. When multiple groups of decoys are launched, the velocity and absolute displacement of the target at each discrimination time can be calculated in advance using (5) to avoid the individual calculation for each module and reduce the complexity of the model.

The motion characteristics of the decoy when launched without maneuvering are shown in Fig. 5.

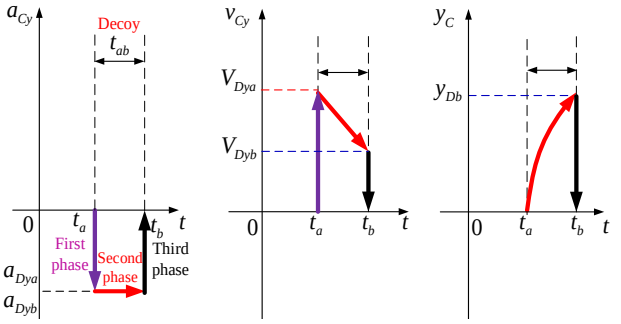

(a) Acceleration variation of power centroid caused by decoy (b) Velocity variation of power centroid caused by decoy (c) Displacement variation of power centroid caused by decoy

Fig. 5 The process of decoy interference

In Fig. 5, the decoy is launched at t_a and discriminated at t_b using the anti-interference algorithm of the seeker. y_{Db} represents the position of the decoy at t_b. In the first phase (t_a), it can be considered that the position of the decoy coincides with the IR radiation source of the target, however the acceleration and velocity of the power centroid change. The acceleration shift value Δa_{Dya} and velocity shift value ΔV_{Dya} caused by the decoy can be calculated using (12). During the second phase (t_a–t_b), because the acceleration of the power centroid caused by the decoy is considered to be constant before, the velocity changes linearly and the displacement changes parabolically. In the last phase (t_b), Δa_{Dyb}, ΔV_{Dyb}, and Δy_{Db} denote the acceleration, velocity, and position shift value of the power centroid caused by decoy, respectively, at t_b, and they can be expressed as follows:

$$\begin{cases} \Delta a_{Dya} = K_D a_{Dya} \\ \Delta V_{Dya} = K_D V_{Dya} \\ \Delta a_{Dyb} = K_D a_{Dyb} \\ \Delta V_{Dyb} = K_D V_{Dyb} \\ \Delta y_{Db} = K_D y_{Db} \end{cases} \tag{12}$$

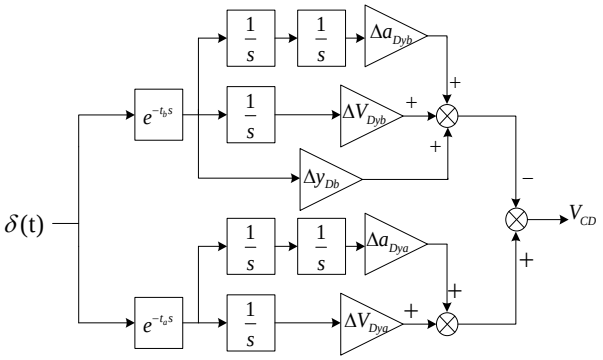

Fig. 6 Motion model of power centroid under decoy interference

Therefore, the linearized model of the power centroid under decoy interference can be expressed as an impulse function, as shown in Fig. 6. In this figure, V_{CD} represents the effect of the decoy on the velocity of the power centroid.

2.4 Calculation model of miss distance for IR decoy in emergency launch mode

The emergency launch mode means that the target will launch decoys intensively with a period of successive launches less than the t_{ab}. Because the t_{ab} is generally small, for the convenience of modeling analysis, it is assumed that the period of successive launches is $t_{ab}/2$. As previously assumed, when a new decoy appears in the seeker's field of view, the seeker needs another time t_{ab} to discriminate the real target. It is assumed that t_{ab} after launch, every decoy will be out of the seeker's field of view or have been eliminated by the anti-interference algorithm. Consequently, the power centroid calculation does not consider these eliminated decoys. The power centroid moves toward the target after the new decoy launches; however, based on previous assumptions, the seeker will continue aiming at the power centroid consisting of the target and multiple new decoys. The seeker will not discriminate the real target for a long period of time, and this increases the discrimination difficulty because of the lack of target information accumulation. Therefore, it is necessary to study the influence of emergency launch mode on the missile miss distance. Table 1 shows the weight coefficients of the power centroid at the time of the first row in the emergency launch mode, so the sum of the coefficients in every column is 1. K_1, K_2, K_3, and K_4 are the weight coefficients of the power centroid and can be calculated as follows:

$$\begin{cases} K_1 = 1/(nK+1) \\ K_2 = nK/(nK+1) \\ K_3 = 1/(2nK+1) \\ K_4 = nK/(2nK+1) \end{cases} \tag{13}$$

Table 1 Weight coefficients of power centroid

Target and decoys	t_{step}	$t_{step}+\frac{t_{ab}}{2}$	$t_{step}+t_{ab}$	$t_{step}+\frac{3t_{ab}}{2}$	⋯	$t_{step}+\frac{mt_{ab}}{2}$
Target	K_1	K_3	K_3	K_3	⋯	K_3
Decoy 1	K_2	K_4	0	0	⋯	0
Decoy 2	0	K_4	K_4	0	⋯	0
Decoy 3	0	0	K_4	K_4	⋱	0
⋮	⋮	⋮	⋮	⋱	⋱	0
Decoy m	0	0	0	0	K_4	K_4

The target launches the first group decoys at t_{step}, and no more than three groups of decoys should be considered when calculating the power centroid. The parameters shown in Table 1 are the weight coefficients of the target and decoy in the power centroid calculation at each time step; therefore, the shift value of each time can be calculated by using the weight coefficients of the current column minus the former ones. We can then establish a mathematical model of the emergency launch mode based on the conventional launch mode.

2.5 Linearized model of IR air-to-air missile

In the linearized model of the missile, the LOS angle q, angular rate $\dot{q}$, and angular acceleration $\ddot{q}$ of the missile can be calculated as:

$$\begin{cases} q = \dfrac{y}{V_C t_{go}} \\ \dot{q} = \dfrac{1}{V_C t_{go}^2}(y + t_{go}\dot{y}) \\ \ddot{q} = \dfrac{1}{V_C t_{go}^3}(2y + 2t_{go}\dot{y} + t_{go}^2\ddot{y}) \end{cases} \tag{14}$$

If the missile adopts TPN, the direction of the missile overload command is vertical to that of the LOS and can be stated as

$$a_{TPN}(t) = NV_c\dot{q} \tag{15}$$

If the missile can estimate the target acceleration value and adopts APN, the overload value of the guidance law output a_{APN} can be expressed as:

$$a_{\mathrm{APN}}(t)=NV_{\mathrm{c}}\dot{q}+\frac{N}{2}a_{\mathrm{T}}(t) \tag{16}$$

a_{APN} can be transformed to the LOS angular acceleration guidance algorithm a_{AAG}[31], which is calculated using $\ddot{q}$ and the actual acceleration of missile a_{My}, as shown in (17). It is undeniable that the differential link will reduce the resistance ability of the system to noise, and as a result, in practical applications, we can estimate $\ddot{q}$ using a Kalman filter and obtain $a_{\mathrm{M}r}$ using the missile inertial navigation system.

$$a_{\mathrm{AAG}}(t)=\frac{N}{2}\left(V_{\mathrm{c}}t_{\mathrm{go}}\ddot{q}+a_{\mathrm{M}r}\right) \tag{17}$$

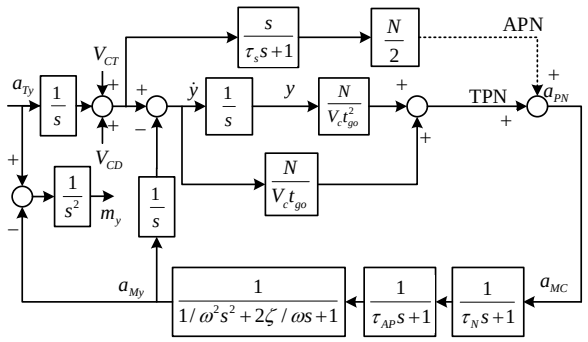

Fig.7 Linearized model of air-to-air missile

Using the superposition principle, taking the *Y*-direction as an example, combined with the calculation module shown in Fig. 4 and Fig. 6, a linearized model of the target barrel roll maneuver with decoy deployment influence on the missile is established, as shown in Fig. 7. τ_{N}, τ_{AP}, ω_{M}, ζ and N are the signal processing time constant, autopilot time constant, airframe response angular velocity, damping ratio, and proportional navigation coefficient of the missile, respectively.

2.6 Establishment of adjoint analysis model

According to the criterion for establishing the adjoint model of the linearized system [4], the adjoint analysis model of the target barrel roll and decoy launch influence on the missile was established. The adjoint form of the time-delay link is itself. The model in this study uses a time-forward simulation to calculate the required parameters of the adjoint model, which can avoid complicated case discussion and parameter derivation, as well as to aid the research on more complex maneuvers, continuous maneuvers, and multiple decoy launches.

There are three inputs in the model shown in Fig. 7; therefore, the miss distance in the *Y*-direction, m_y, is the sum of the three outputs. Similarly, the miss distance in the *Z*-direction (m_z) can be acquired, and the miss distance m_{all} can be expressed as:

$$m_{\mathrm{all}}=\sqrt{m_y^2+m_z^2} \tag{18}$$

For the multi-decoy case, the shift value calculation module can be connected in parallel with the missile adjoint model at the corresponding time. Furthermore, through one simulation of the adjoint method, we can obtain the results of the time-forward system, which needs to be simulated many times; that is, the calculation efficiency is greatly improved.

3 Simulation and analysis

3.1 Time-forward model validation

Compared with the adjoint model, each variable of the time-forward simulation model has a clear physical significance and is easy to follow. Therefore, the time-forward simulation model was validated by taking the barrel roll maneuver and one decoy launch for the TPN missile as an example. The simulation conditions are listed in Table 2. The acceleration changes in the power centroid induced by the target and decoy, the acceleration of the target, and the power centroid are shown in Fig. 8, and the corresponding velocity and position changes are shown in Fig. 9 and 10. At 0.4 s, the target implements a barrel roll maneuver and launches decoys towards the outside of the circular motion at the same time; meanwhile, the acceleration, velocity, and displacement of the power centroid induced by the maneuver become 1/3 of the target. At 0.8 s, the seeker discriminates the real target, and the physical quantities curve of the power centroid coincides with the target later. All these simulation results match the expected results.

Table 2 Simulation parameters

Symbol/unit	Values	Symbol/unit	Values
$t_{\max}$/s	7	ζ	0.707
τ_{SH}/s	0.11	N	3.5
τ_{N}/s	0.1	V_{c}/(m/s)	1200
τ_{AP}/s	0.14	t_{ab}/s	0.4
ω_{M}/(rad/s)	19	ϕ_0/deg	45

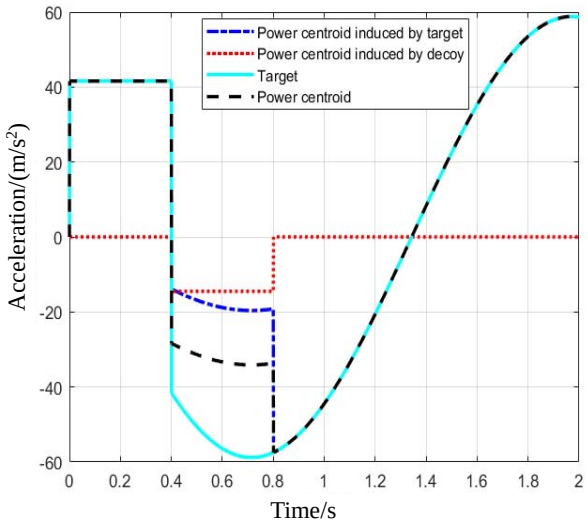

Fig. 8 Acceleration change of the power centroid and the target in the *Y*-direction

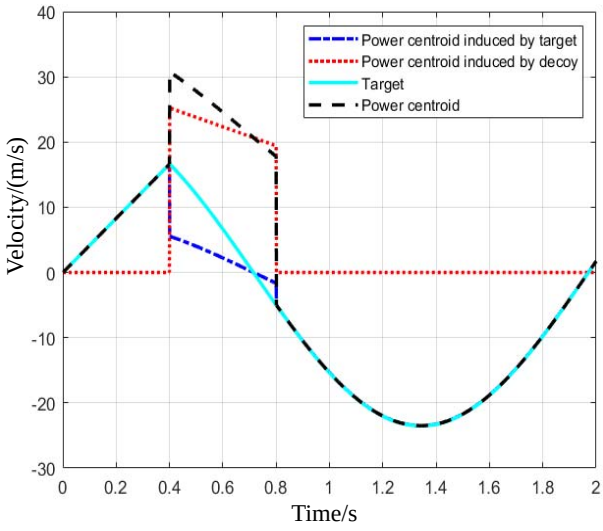

Fig. 9 Velocity change of the power centroid and the target in the *Y*-direction

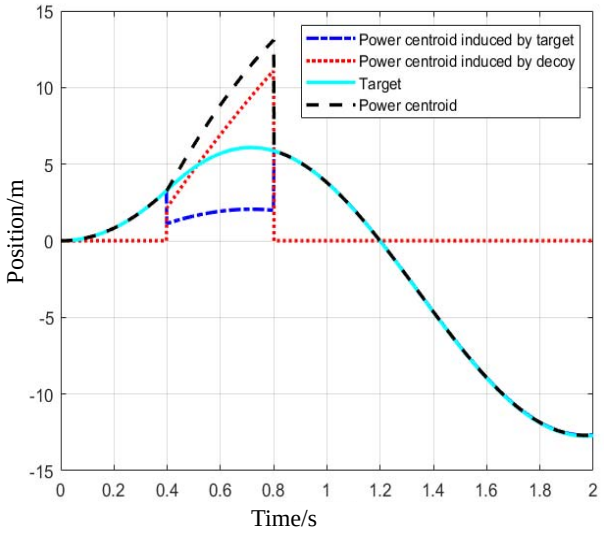

Fig. 10 Position change of the power centroid and the target in the *Y*-direction

3.2 Time-forward simulation and adjoint simulation results validation

All decoys are launched towards the outside of the circular motion, and the time-forward simulation time varies from 0.2 s to 7 s with an interval of 0.2 s. It can be seen from Fig. 11 that the time-forward simulation and the adjoint simulation miss distance exactly coincide, which verifies the correctness of the adjoint model.

3.3 Simulation results of decoy launch during target barrel roll maneuver

The target launches decoys during the barrel-roll maneuver process. The initial mass of a typical decoy is 0.3 kg, the mass consumption rate is 0.04 kg/s, the windward area S is 0.003 m^2, drag coefficient C_d is 0.35, the combustion time is 5 s, and the launch speed is 30 m/s, which is launched upward vertically relative to the target. At the beginning of the simulation, the attitude angles of the target aircraft were all 0 °, the flight altitude was 4 km, the overload was 6 g, the speed is 0.8 Ma, and the barrel roll rate was 2 rad/s. Then, the velocity of the decoy can be obtained. The position of the decoy can be obtained by integrating the velocity. The phase angle of the target barrel roll varied from 0° to 300° at intervals of 60°. The *OYZ* plane trajectory diagram and change in velocity versus time are shown in Fig. 12. The position, velocity, and acceleration of the decoy launched at each moment with different initial phase angles of the barrel roll maneuver were calculated.

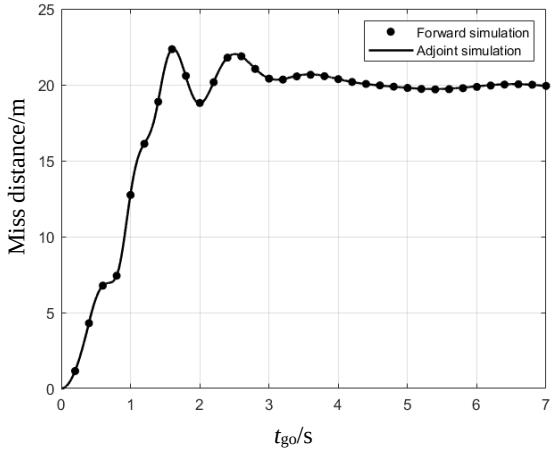

Fig. 11 Miss distance comparison for time-forward simulation and adjoint simulation

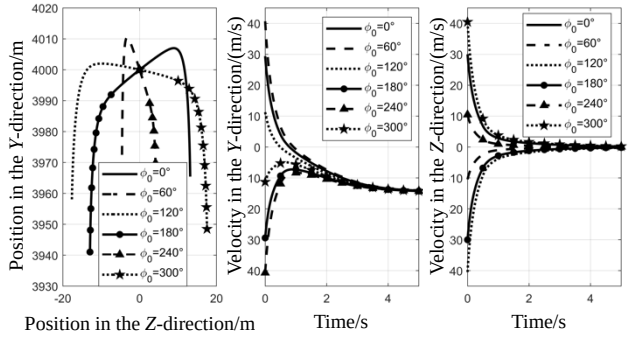

(a) The *OYZ* plane trajectory diagram (b) Velocity in the *Y*-direction vs time (c) Velocity in the *Z*-direction vs time

Fig. 12 The trajectory diagram and the change of velocity vs time

3.4 Analysis of miss distance affected by barrel roll

1) Effect of barrel roll rate on miss distance for TPN and APN missiles

The barrel roll rate ω values studied were 1, 1.5, 2, 3 and 4 rad/s with different associated barrel diameters. The missile was a tail chase on the target, and the remaining simulation parameters were set as listed in Table 2. The influence of the barrel roll rate on the miss distance of the missile was studied. The variation in the missile miss distance versus t_{go} is shown in Fig. 13.

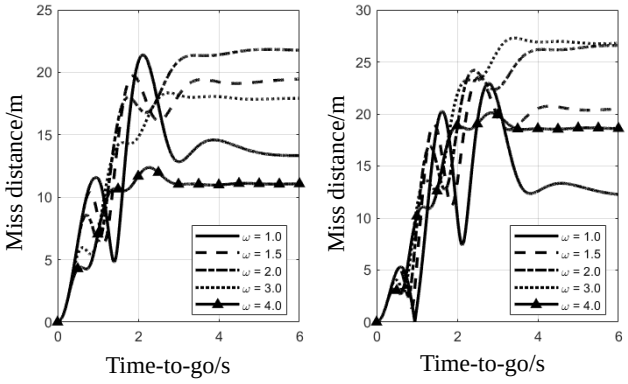

(a) TPN (b) APN

Fig. 13 The variation curves of miss distance vs t_{go} for different barrel roll rates

Suppose that the number of curves for the miss distance versus t_{go} to be compared is l. To facilitate research, the average miss distance $\bar{m}_j$ for the j-th curve is introduced as follows:

$$\bar{m}_j = \frac{1}{t_{\max}} \int_0^{t_{\max}} m_j(t_{go}) \mathrm{d}t_{go} \tag{19}$$

where $t_{\max}$ represents the maximum t_{go} and $m_j(t_{go})$ represents the miss distance corresponding to t_{go}, as shown in Fig. 14 (a). Meanwhile the concept of namely the percentage of the maximum miss distance [25] p_j for the j-th curve can be calculated as:

$$\begin{cases} p_j = \dfrac{1}{t_{\max}} \displaystyle\int_0^{t_{\max}} [1 - \mathrm{sgn}(\max(t_{go}) - m_j(t_{go}))] \mathrm{d}t_{go} \\ \max(t_{go}) = \max(m_1(t_{go}), \cdots, m_j(t_{go}), \cdots, m_l(t_{go})) \end{cases} \tag{20}$$

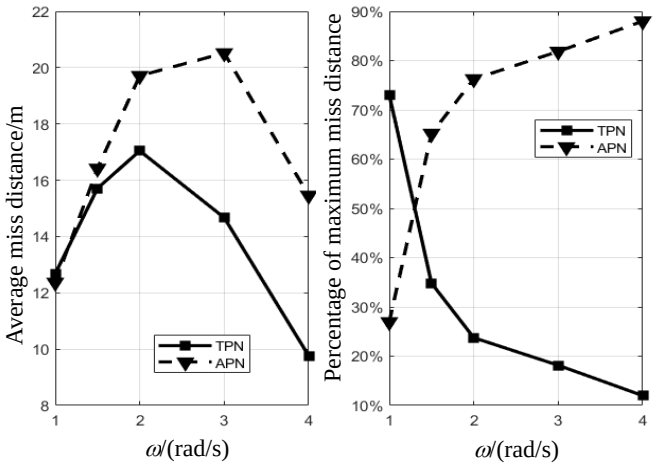

(a) Average miss distance vs ω (b) Percentage of maximum miss distance vs ω

Fig. 14 Analysis of the average miss distance and the percentage of the maximum miss distance

where max(t_{go}) represents the maximum miss distance of all curves corresponding to t_{go}, as shown in Fig. 14(b). Assuming that the probability of each t_{go} under real airborne combat condition is equal, combined with the t_{go} estimation error [32], the higher value means that there will be a greater survival probability. If the average miss distance varies slightly, more useful information can be obtained through the percentage of the maximum miss distance.

It can be seen from Fig. 13 that to make the miss distance generated by the TPN-and APN-guided missiles sufficiently large, the barrel roll maneuver should be performed when t_{go} is greater than 2 s, and the aircraft should try to put the missile behind the tail to increase t_{go}. By combining Fig. 13 and Fig. 14, it can be concluded that with the same barrel roll rate, APN will produce a higher miss distance than TPN. However, when the barrel roll rate is small, the average miss distances of the two guidance laws are not significantly different, nevertheless the TPN will produce a higher miss distance with a higher probability. TPN generates the maximum average miss at approximately 2 rad/s, and APN generates the maximum average miss at 3 rad/s.

2) The influence of initial phase angle of barrel roll maneuver on missile miss distance

The barrel roll rate is set to 2.5 rad/s and decoys are launched vertically upward relative to the target. Two decoys were launched simultaneously with a launch period of 0.6 s. The average miss distance and the percentage of maximum miss distance corresponding to the initial phase angle of the target barrel roll maneuver are shown in Fig. 15. It can be seen that the average miss distances change only slightly with ϕ_0 in this simulation. When ϕ_0 is 0°, the TPN guidance law has the highest percentage of maximum miss distance, whereas when ϕ_0 is 120° and 220°, the TPN guidance law has the highest percentage of maximum miss distance.

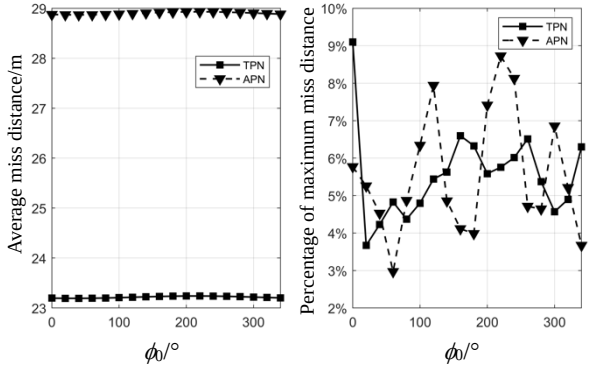

(a) Average miss distance (b) Percentage of maximum miss distance

Fig. 15 Average miss distance and percentage of maximum miss distance vs initial phase angle of barrel roll maneuver

3.5 Analysis of the influence of decoy parameters on miss distance during barrel roll maneuver

1) The influence of simultaneous launch quantity on miss distance

The parameters of the decoy launch and barrel roll rate were set as shown in Fig. 12 and 15. The other parameters are the same as those shown in Fig. 13. The initial phase angle of the barrel roll maneuver was 0°. The suppression coefficient for one decoy was set to 2, and the suppression ratio K for the simultaneous launch quantity n decoys was $2n$. The variation curve of the miss distance versus t_{go} is shown in Fig. 16, where K=0 indicates that no decoy was launched.

As shown in Fig. 16, for the two types of guidance laws, more simultaneous launches lead to higher missile miss distances. Comparing the curves in the figure, the decoy launch generates a higher miss distance than merely implementing barrel roll; however, with the increase in quantity, the miss distance growth tendency decreases. Furthermore, because of the limited quantity of decoys carried on the aircraft and the fact that there are generally multiple missile attacks during airborne combat, the simultaneous launch quantity should not be set higher than two or three due to economic and efficacy concerns.

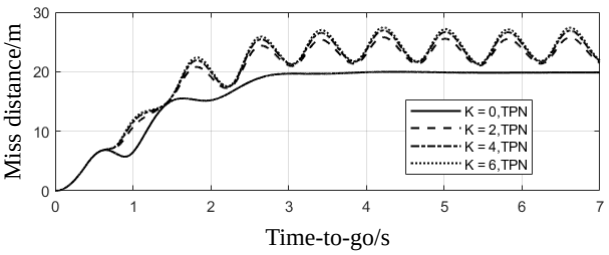

(a) Miss distance vs time-to-go for TPN

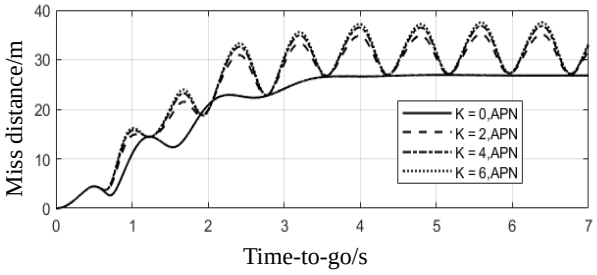

(b) Miss distance vs time-to-go for APN

Fig. 16 Miss distance vs t_{go} for different simultaneous launch quantity

2) The influence of the period between successive launches and launch direction policy on missile miss distance

The most practical deployment of decoys is to launch them at a certain rate [29]. The group time intervals for conventional launch mode are from 0.5 s to 2.1 s with an interval of 0.2 s, while for emergency launch mode it is set to 0.2 s. The simultaneous launch quantity is 2, and the barrel roll rate is 2.5 rad/s. Here, considering four policies, decoys are launched in the same directions for the first two policies, while for each of the other two policies, decoys are launched in reverse directions. The first group of decoys for the first and third policies are launched towards the outside of the circular motion, whereas for the other two policies, decoys are launched towards the inside. The remaining simulation conditions were the same as those shown in Fig. 15. The launch speeds of all the decoys were the same, and the initial phase angle of the barrel roll was 0 °. The average miss distance of the missile in the emergency launch mode is shown in Table 3; the influence on the miss distance under different

launch policies in the conventional launch mode is shown in Fig. 17.

By comparing Table 3 and Fig. 17, it can be seen that the emergency launch mode generates a higher average miss distance, which is likely to cause the target to fly out of the seeker field of view to complete the escape.

Table 3 The average miss of missile in the emergency launch mode

Guidance law	First policy	Second policy	Third policy	Fourth policy
TPN	85.55	99.57	92.10	92.29
APN	87.28	103.71	94.71	95.01

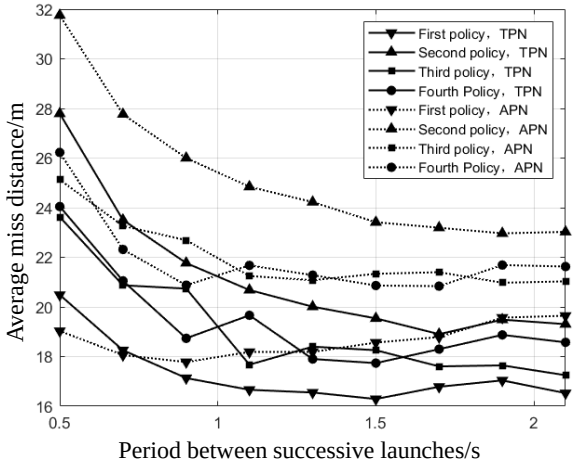

Fig. 17 The variation curve of the average miss distance under different launch policies in conventional launch mode

It can be concluded from Fig. 17 that under the same launch policy, the target will generate a higher average miss distance for missiles guided by the APN compared with the TPN. The first and second policies led to the minimum and maximum miss distances, respectively, and the other two policies were in between. Furthermore, when the period between successive launches is less than 1 s, the average miss distance for all policies decreases significantly with an increase in the period, and when it is greater than 1 s, the influence of the launch period on the average miss distance of the missile decreases.

4 Conclusions

In this study, a realistic target barrel roll maneuver model, decoy launch model, and adjoint analysis model were established for missile guidance accuracy. The influence of the target barrel roll maneuver and IR decoy on the miss distance of the IR-guided missile was studied. After the missile warning system issues an alarm signal, the target should place the missile behind the tail and implement a step maneuver with the maximum overload. When the velocity condition is reached, the target will perform the barrel roll maneuver with a roll rate of approximately 2 rad/s for TPN-guided missiles and with a roll rate of approximately 3 rad/s for APN-guided missiles. Currently, the aircraft launches decoys outside of the circular motion. The proposed simultaneous launch quantity is 2 or 3, and the period between successive launches should be less than 1 s. If necessary, an emergency launch mode can be implemented for great effect. This study has significance in providing guidance on target maneuvers and decoy launches for evading IR-guided missiles.

References:

[1] Raghav Harini Venkatesan, Nandan Kumar Sinha. Key factors that affect the performance of flares against a heat-seeking air-to-air missile[J]. *The Journal of Defense Modeling and Simulation*: *Applications, Methodology, Technology*, 2014, **11**(4): 387-401.

[2] Giovanni Franzini, Luca Tardioli, Lorenzo Pollini, et al. Visibility augmented proportional navigation guidance[J]. *Journal of Guidance, Control, and Dynamics*, 2018, **41**(4): 983-991.

[3] XU Yang, FANG Yangwang, WU Youli, et al. Proportional guidance intelligent regulation strategy under the infrared interference and maneuvering[J]. *Journal of National University of Defense Technology*, 2019, **41**(3): 137-145.

[4] Paul Zarchan. *Tactical and strategic missile guidance*[M]. the 6th, AIAA, 2012.

[5] WANG Xiaohai, MENG Xiuyun, ZHOU Feng, et al. Sliding mode guidance law with impact angle constraint based on bias proportional navigation[J]. *Systems Engineering and Electronics*, 2021, **43**(5): 1295-1302.

[6] LI Kebo, LIANG Yangang, SU Wenshan, et al. Performance of 3D TPN against true-arbitrarily maneuvering target for exoatmospheric interception[J]. *Science China Technological Sciences*, 2018, **61**(8): 1161-1174.

[7] LEE Suwon, LEE Youngjun, LEE Seokwon, et al. Data-driven capturability analysis for pure proportional navigation guidance considering target maneuver[J]. *International Journal of Aeronautical and Space Sciences*, 2021,**22**(5): 1209-1221.

[8] LI Kebo, LIAO Xuanping, LIANG Yangang, et al. Guidance strategy with impact angle constraint based on pure proportional navigation[J]. *Acta Aeronautica et Astronautica Sinica*, 2020, **41**(S2): 724277.

[9] Satadal Ghosh, Debasish Ghose, Soumyendu Raha. Composite guidance for impact angle control against higher speed targets[J]. *Journal of Guidance, Control, and Dynamics*, 2016, **39**(1): 98-117.

[10] LI Kebo, LIANG Yangang, SU Wenshan, et al. Performance of 3D TPN against true-arbitrarily maneuvering target for exoatmospheric interception[J]. *Science China Technological Sciences*, 2018, **61**(8): 1161-1174.

[11] FENG Tyan. The capture region of a general 3D TPN guidance law for missile and target with limited maneuverability[C]//*Proc. American Control Conference*, 2001: 512-517.

[12] BAI Zhihui, LI Kebo, SU Wenshan, et al. Capture region of RTPN guidance law against arbitrarily maneuvering targets[J]. *Acta Aeronautica et Astronautica Sinica*, 2020, **41**(8): 323947.

[13] SHI Zhenqing, LIANG Xiaolong, ZHANG Jiaqiang, et al. Modeling and simulation analysis of 3-D air-to-air missile attack zone under the condition of target maneuvers[J]. *Journal of Projectiles, Rockets, Missiles and Guidance*, 2019, **39**(3): 97-106.

[14] Ernst-Christian Koch. Review on pyrotechnic aerial infrared decoys[J]. *Propellants, Explosives, Pyrotechnics*, 2011, **26**(1): 3-11.

[15] Ilan Rusnak. Bounds on the root-mean-square miss of radar-guided missiles against sinusoidal target maneuvers[J]. *Journal of Guidance, Control, and Dynamics*, 2011, **34**(4): 1066-1069.

[16] Fumiaki Imado and Sachio Uehara. High-g barrel roll maneuvers against proportional navigation from optimal control viewpoint[J]. *Journal of Guidance, Control, and Dynamics*, 1988, **21**(6): 876-881.

[17] Timo Sailaranta, Ari Siltavuori, Antti Pankkonen. Simple missile models against high-g barrel roll maneuver[C]//*Proc. AIAA Guidance, Navigation, and Control Conference*, 2011: 01-12.

[18] Ernst Christian Koch, Arno Hahma, Volker Weiser, et al. Metal-Fluorocarbon Pyrolants. XIII: High performance infrared decoy flare compositions based on MgB_2 and Mg_2Si and polytetrafluoroethylene/viton[J]. *Propellants Explosives Pyrotechnics*, 2010, **35**: 1-7.

[19] Srinivasan Ramaswam, David A Vaitekunas, Willem H Gunter, et al. Improvements to the ShipIR/NTCS adaptive track gate algorithm and 3D flare particle model[C]//*Proc. SPIE Defense + Security*, 2017, **10178**: 1-12.

[20] LI Shaoyi, ZHANG Kai, YIN Jianfei, et al. Study on IR target recognition approach in aerial jamming environment based on bayesian probabilistic model[J]. *IEEE Access*, 2019, **7**: 50300-50316.

[21] SHI Chen. Research on target recognition for anti-jamming towards infrared decoys[D]. Chengdu: University of Electronic Science and Technology of China, 2020.

[22] Martin Weiss. Adjoint method for missile performance analysis on state space models[J]. *Journal of Guidance, Control and Dynamics*, 2005, **28**(2): 236-248.

[23] Martin Weiss, Domenic Bucco. Adjoint method for hybrid guidance loop state-space models[J]. *Journal of Guidance, Control, and Dynamics*, 2015, **38**(4): 614-622.

[24] Martin Weiss, Domenic Bucco. Evaluation method for dual phase guided weapons based on the adjoint method[C]//*Proc. AIAA Guidance, Navigation and Control Conference and Exhibit*, 2007: 1-12.

[25] LI Quancheng, FAN Yonghua, WAN Shizheng, et al. Influence of the seeker blind range guidance policy on guidance precision[C]//*Proc. IEEE 9th Annual International Conference on CYBER Technology in Automation, Control, and Intelligent Systems* (CYBER), 2019: 1120-1124.

[26] Vitaly Shalumov, Tal Shima. Weapon–target-allocation strategies in multiagent target–missile–defender engagement[J]. *Journal of Guidance, Control and Dynamics*, 2017, **40**(10): 2452-2464.

[27] Domenic Bucco and Martin Weiss. Blind range influence on guidance loop performance: an adjoint-based analysis[C]//*Proc. AIAA Guidance, Navigation, and Control Conference*, 2013: 1-16.

[28] WANG Weiqiang, JIA Xiaohong, FU Kuisheng, et al. Guidance precision analysis based on airborne IRCM stochastic process[J]. *Infrared Technology*, 2019, **41**(2): 163-170.

[29] Arthur Vermeulen, Gerrit Maes. Missile avoidance maneuvres with simultaneous decoy deployment[C]//*Proc. AIAA Guidance, Navigation, and Control Conference*, 2009: 1-17.

[30] HUANG Hesong, TONG Zhongxiang, LI Taorui, et al. Defense strategy of aircraft confronted with IR guided missile[J]. *Mathematical Problems in Engineering*, 2017, **2017**: 1-9.

[31] Hecht C. Homing guidance using angular acceleration of the line of sight[C]//*Proc. Navigation & Control Conference*, 1991: 856-869.

[32] Satadal Ghosh, Debasish Ghose, Soumyendu Raha. Unified time-to-go algorithms for proportional navigation class of guidance[J]. *Journal of Guidance, Control and Dynamics*, 2016, **39**(6): 1188-1205.